

Under-ice acoustic navigation using real-time model-aided range estimation

EeShan C. Bhatt,^{1, 2, a} Oscar Viquez,² and Henrik Schmidt²

¹*MIT-WHOI Joint Program in Oceanography/Applied Ocean Science & Engineering,
Cambridge and Woods Hole, MA, USA*

²*Department of Mechanical Engineering, Massachusetts Institute of Technology,
Cambridge, MA*

(Dated: 20 February 2022)

1 The long baseline (LBL) underwater navigation paradigm relies on the conversion
2 of recorded travel times into pseudoranges to trilaterate position. For real-time op-
3 erations, this conversion has assumed an isovelocity sound speed. For re-navigation
4 in post-processing, computationally and/or labor intensive acoustic modeling may
5 be employed to reduce uncertainty driven by multipath arrivals. This work demon-
6 strates a real-time ray-based prediction method of the effective sound speed along
7 a path from source to receiver to minimize vehicle position error. This method was
8 implemented for a small scale AUV-LBL system in March 2020, in the Beaufort Sea,
9 in total ice-covered conditions and a double ducted acoustic propagation environ-
10 ment. The vehicle was successfully deployed and recovered. Given the lack of GPS
11 data throughout the vehicle’s mission, however, the pseudorange performance is first
12 evaluated on connections between GPS-linked beacons. The real-time ranging error
13 between beacons is roughly 11 meters at distances up to 3 km. But a consistent over-
14 estimation in the real-time method provides insights for improved eigenray filtering
15 by the number of surface bounces. An operationally equivalent pipeline is used to
16 re-position the LBL beacons and re-navigate the AUV, using a modeled, historical,
17 and a locally observed sound speed profile. The median re-navigation error is 1.84 ± 2.19 RMS m. The improved trilateration performance for suggests that this ap-
18 proach effectively extends the single meter accuracy of the deployed GNSS units into
19 the water column.

^aebhatt@whoi.edu

²¹ **I. INTRODUCTION**

²² Autonomous underwater vehicles (AUVs) are increasingly capable platforms to explore
²³ and sample the ocean, particularly for remote and/or dangerous regions. However, navi-
²⁴ gation uncertainty is a major challenge in considering AUVs as standard tools for oceano-
²⁵ graphic research. While land and air-based robots utilize information from Global Naviga-
²⁶ tion Satellite Systems (GNSS) to achieve stunning location accuracy and precision through-
²⁷ out the duration of their missions, AUVs cannot access GNSS fixes while underwater. There-
²⁸ fore, underwater vehicles have relied on any combination of dead reckoning, hydrodynamic
²⁹ models, inertial navigation systems, doppler velocity logs, and acoustic baseline positioning
³⁰ systems for navigation (Paull *et al.*, 2014). Limiting navigation error and drift requires an
³¹ AUV to periodically stall on the surface and obtain a GNSS fix to reset its position error.
³² This foolproof method of self-positioning is undesirable for stealth, adverse weather condi-
³³ tions, and mission efficiency, and inaccessible in a GNSS-denied situation like an ice-covered
³⁴ environment.

³⁵ Of underwater acoustic navigation systems, long baseline (LBL) is the most GPS-like
³⁶ in style and scale, and most appropriate for mitigating drift without overburdening com-
³⁷ putation or payload size on the vehicle (Van Uffelen, 2021). The state-of-the-art for LBL
³⁸ outsources depth to a pressure sensor and solves the two-dimensional localization problem
³⁹ with an isovelocity, linear scaling between one way travel time (OWTT) and range (Eustice
⁴⁰ *et al.*, 2006, 2007; Webster *et al.*, 2009, 2012). This assumption is valid for short scale
⁴¹ operations but oversimplifies propagation for larger and/or complex acoustic environments.

42 To achieve single meter, GNSS-like performance in a GNSS-denied environment, we demon-
 43 strate an embedded ray-based data processing algorithm to convert recorded OWTTs into
 44 pseudorange estimates. This methodology was integrated onto the AUV *Macrura*, deployed
 45 and recovered in the Beaufort Sea, in March 2020, during the Ice Exercise 2020 (ICEX20).
 46 A physics-driven methodology that received an *in situ* sound speed profile (SSP) was nec-
 47 essary despite the small operational domain because of the relatively high-risk mission en-
 48 vironment—total under-ice conditions and a variable double ducted acoustic environment.
 49 For consistency, we delineate specific definitions for timing, positioning, and navigation
 50 from [Howe et al. \(2019\)](#).

- 51 1. Timing is the ability to acquire and maintain accurate and precise time anywhere in
 52 the domain of interest within user-defined timeliness parameters
- 53 2. Positioning is the ability to accurately and precisely determine one's location refer-
 54 enced to a standard geodetic system
- 55 3. Navigation is the ability to determine current and desired position (relative or absolute)
 56 and apply corrections to course, orientation, and speed to attain a desired position
 57 anywhere in the domain of concern

58 Thus, navigation is inherently in real-time and depends on positioning; positioning depends
 59 on timing. We also suggest re-navigation and re-positioning as post-processed corollaries,
 60 which may include knowledge or processing capabilities not available *in situ*.

61 While RAFOS floats championed one way ranging for re-positioning ([Duda et al., 2006](#);
 62 [Rossby et al., 1986](#)), the ability to do so for navigation was facilitated by the advent of

the WHOI Micro-Modem (Singh *et al.*, 2006) and synchronized clocks (Rypkema *et al.*, 2017). AUV navigation efforts have achieved root mean square (RMS) localization error on the order of tens of meters relative to GNSS surface position over less than ten kilometers in shallow (Claus *et al.*, 2018; Eustice *et al.*, 2007; Kepper *et al.*, 2017) and deep water (Jakuba *et al.*, 2008; Kunz *et al.*, 2008; Webster *et al.*, 2009). However, these efforts all used a nominal sound speed for travel time conversion and the vehicles were limited to shallower isovelocity regimes.

Localization algorithms that do consider environmental or acoustic uncertainty tend to focus on longer and larger experiments, where spatio-temporal variability cannot be ignored. These methods have also been reserved for post-processing as they can be labor intensive, computationally heavy, and/or require additional information like contemporaneous data. For example, gliders navigating with kinematic flight models and equipped with acoustic modems were later unambiguously associated with predicted ray arrivals, resulting in roughly a kilometer error and hundred meters uncertainty over basin scale propagation (Van Uffelen *et al.*, 2013). A follow up study investigated how a single temporally and spatially averaged SSP could mitigate position error for a four month glider mission (Uffelen *et al.*, 2016). Wu *et al.* (2019) cross correlate three days of real acoustic records with synthetic ones generated through ocean model snapshots from HYCOM (Chassagnet *et al.*, 2007). While potentially applicable for various ocean states, this is reliant on model realism and impractical for real-time operations. Mikhalevsky *et al.* (2020) introduces a “cold start” algorithm that does not require prior knowledge of track, position, or sound speed information. The algorithm inputs a four-dimensional ocean model, constrained by tomography data, into a range dependent

85 ray code to isolate the last path detected in a full multipath pattern. Then, a representative
86 group speed is solved for alongside position in a least squares fashion. This approach is able
87 to re-position a floating hydrophone array with an error of 58 m and a standard deviation
88 of 32 m based on six sources 129–450 km away but remains to seen for real-time navigation.

89 The ICEX20 AUV deployment necessitated an environmentally- and physically-driven
90 relationship between recorded travel times and estimated pseudoranges due to the multipath
91 uncertainty brought upon by an increasingly observed double ducted environment in the
92 Beaufort Sea, which some refer to as the “Beaufort Lens” (Chen *et al.*, 2019; Chen and
93 Schmidt, 2020; Litvak, 2015).

94 Given that a lens introduces significant ray refraction, the Beaufort Lens is a shorthand for
95 the spatio-temporal variability of the local temperature and sound speed maxima generally
96 around 50 to 60 m in depth. A neutrally buoyant layer of warm Pacific Summer Water
97 creates a unique double ducted environment —the upper duct degrades signal coherence
98 due to intensified ice interaction and the lower duct effectively traps sound for long range
99 propagation (Poulsen and Schmidt, 2017). Modeling output (Duda *et al.*, 2021, 2019) and
100 experimental observations (Ballard *et al.*, 2020; Bhatt, 2021) suggest that, in the Beaufort
101 Sea, the duct is persistent and widespread but not necessarily continuous; it and its acoustic
102 effects can be non-existent, minimal, or drastic. Transmissions in the upper duct, between
103 the surface ice and the lens, experience minimal attenuation but degrade in signal coherence
104 with repeated reflections under the ice. In lower duct, between the lens and its conjugate
105 depth in the Atlantic water, roughly 200 m, sound above 350 Hz is trapped near losslessly
106 for long range propagation (Poulsen and Schmidt, 2017).

107 Thorough reviews of uncrewed vehicle operations in polar environments can be found in
108 (Norgren *et al.*, 2014) and (Barker *et al.*, 2020); there is no comparable work in the Arctic
109 for a short range AUV deployment in the Beaufort Lens. Seminal (Bellingham *et al.*, 1995;
110 Brooke, 1981; Hayes and Morison, 2002; Jackson, 1983; Light and Morison, 1989) and more
111 recent AUV deployments (Fossum *et al.*, 2021; Jakuba *et al.*, 2008; Kukulya *et al.*, 2010;
112 Kunz *et al.*, 2008; Plueddemann *et al.*, 2012; Timmermans and Winsor, 2013) witnessed the
113 classical upward refracting sound speed profile that is amenable to an isovelocity assumption.

114 Of note, despite different platforms and scales, are recent glider deployments in the
115 Canada Basin. In 2014, in partially ice-covered conditions, a long range LBL system with
116 WHOI Micro-Modems at 100 m exploited the lower duct for long range communication with
117 two gliders (Freitag *et al.*, 2016; Webster *et al.*, 2015). The sound speed value measured at
118 the time of reception was used to estimate pseudorange in post-processing. The beacon-to-
119 beacon performance was excellent, achieving contact at ranges greater than 200 km with
120 a position uncertainty of 40 m. The beacon-to-glider performance, however, deteriorated
121 due to missed contacts outside the duct, and was not described quantitatively. In 2017,
122 gliders were deployed in a region with no ice coverage (Graupe *et al.*, 2019). Ranges were
123 linearly scaled by a statistical description of sound speed observations taken during the
124 experiment, 1450 ± 6.5 m/s. This resulted in an error of 550 m, which was reduced by
125 a factor between 4 and 5, depending on the dive, using a post-processing acoustic arrival
126 matching method. Both cases exploit the lower duct for high fidelity communication at
127 long ranges. Unintuitively, the smaller nature of our deployment during ICEX20 is not a

¹²⁸ simplifying factor. For source depths typical to vehicle operations, 30 to 200 m, a shadow
¹²⁹ zone spans from 2 to 6 kilometers in range ([Schmidt and Schneider, 2016](#)).

¹³⁰ Compared to the previous small scale navigation efforts, the approach in this paper
¹³¹ integrates real-time model-aided data processing to estimate a representative sound speed
¹³² along a path from source to receiver, leveraging climatology, *in situ* data, and fast acoustic
¹³³ modeling. The paper is organized as follows. Section [II](#) details the experimental approach
¹³⁴ and conditions during ICEX20. Given that there is no GNSS ground truth for the vehicle
¹³⁵ position while underway, we first evaluate the real-time ranging performance of GPS-linked
¹³⁶ beacon-to-beacon communication events in section [III](#). Section [IV](#) uses insights from field
¹³⁷ data to introduce a new ray filtering algorithm to improve range estimation. Section [V](#)
¹³⁸ emulates the real-time processing pipeline to re-position beacon-to-beacon events and re-
¹³⁹ navigate AUV *Macrura*.

¹⁴⁰ **II. OVERVIEW OF THE ICEX20 EXPERIMENT**

¹⁴¹ The results from this paper derive from data taken while deploying the AUV *Macrura*, a
¹⁴² custom Bluefin-21, during the Ice Exercise 2020 (ICEX20), in the Beaufort Sea, from March
¹⁴³ 8th to 11th. The AUV deployment was supported by the Integrated Communication and
¹⁴⁴ Navigation Network (ICNN) ([Randeni et al., 2020, 2021; Schneider et al., 2020](#)), a special-
¹⁴⁵ ized implementation of the LBL solution. The ICNN was initially developed via numerous
¹⁴⁶ virtual experiments to ensure robust algorithms and interfaces between different hardware
¹⁴⁷ components. The simulation capabilities are largely physics-driven with a modular system of
¹⁴⁸ systems approach—an environmental simulator with sub-components for the ocean, includ-
¹⁴⁹ ing Arctic ice drift and ocean acoustic propagation; a vehicle simulator with sub-components
¹⁵⁰ for vehicle dynamics and navigation; a topside hardware simulator and acoustic communica-
¹⁵¹ tions simulator, both with a software-only configuration and a hardware-in-the-loop version
¹⁵² ([Schneider and Schmidt, 2018](#)). The virtual environment similarly emulates the interfaces
¹⁵³ between the real components to test the entire software pipeline.

¹⁵⁴ **A. The Integrated Communication and Navigation Network**

¹⁵⁵ The ICNN is comprised of four ice buoys in a loose rectangle, roughly 2 km away from
¹⁵⁶ a central ice camp with a topside computer, as shown in Fig. 1. Each ice buoy is outfitted
¹⁵⁷ with a Garmin GPS 18x, with a pulse-per-second rising edge aligned to 1 microsecond and
¹⁵⁸ a spec sheet accuracy of 3 m, 95% of the time. The AUV and each ice buoy are outfitted
¹⁵⁹ with a WHOI Micro-Modem ([Singh et al., 2006](#)), with a four-element receiver array, a single

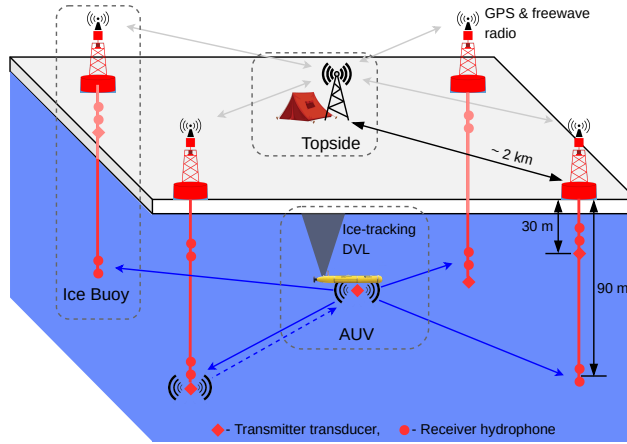


FIG. 1. A schematic overview of the Integrated Communication and Navigation Network (ICNN), which provides joint data-transfer and tracking between AUV and a human decision maker at Topside.

160 transmitter, and one-tenth of a millisecond resolution. Acoustic messages were sent with
 161 a 10 kHz carrier frequency, 5 kHz bandwidth, and phase-shift keying (PSK) modulation on
 162 a time-division multiple access schedule with a thirty-second cycle, giving room for two-
 163 way communication throughout the mission volume. The receive and transmit elements
 164 were split between shallow and deeper depths—30 and 90 m—to provide better coverage
 165 across the shadow zone. While each buoy only has one transmit depth, all buoys have both
 166 receive depths but the active receive layer is consistent across all buoys. The design of
 167 the ICNN enables a self-adapting network to transmit and receive at the optimal depth to
 168 maintain contact with the AUV ([Schneider et al., 2020](#)). The buoys do not encompass the
 169 full horizontal range of the vehicle but are positioned to minimize overlap in trilateration
 170 for spherical positioning ([Deffenbaugh et al., 1996a](#)).

171 To balance competing uses of the acoustic channel, the network uses a single synchronized

172 digital communication packet to provide both tracking and data to the operator.

173 1. The AUV, running an ice-tracking DVL and an onboard hydrodynamic model, broad-

174 casts its perceived location on a scheduled, time-synchronized message via WHOI

175 Micro-Modem

176 2. Four ice buoys, each outfitted with a WHOI Micro-Modem, receive messages from the

177 AUV and send that information over freewave radio to a Topside computer

178 3. The topside computer converts travel times into pseudorange estimates using a stochas-

179 tic embedded prediction of the horizontal group velocity via BELLHOP ray tracing

180 code ([Porter, 2011](#)) using a sound speed profile provided by an updatable Virtual

181 Ocean ([Bhatt et al., 2022; Schneider and Schmidt, 2018](#))

182 4. The topside computer calculates a new position by trilaterating the range estimates

183 5. The position differential, not the absolute position, is broadcast to the vehicle to

184 update its navigation solution and be robust to latency and intermittency

185 In the face of GNSS-denied navigation, this approach was anecdotally successful, as shown

186 in Fig. 2. The AUV *Macrura* was deployed through a hydrohole from an ice camp but re-

187 covered through an emergency hydrohole. A random disk error stalled *Macrura* underneath

188 the ice but did not prevent it from transmitting its location. Due to an incoming storm, a

189 team placed a physical marker on the ice at the location. Three days later, *Macrura* was

190 found within a meter of the marker. We view the emergency recovery as qualitative proof

191 of the robustness of this navigation approach. Nonetheless, this paper specifically addresses

the third and fourth steps—the conversion of travel times into pseudoranges and its effect on trilateration. By focusing on pseudorange estimates between GPS-tracked beacons, and re-running the trilateration pipeline, the results are decoupled from all other mechanisms in the ICNN.

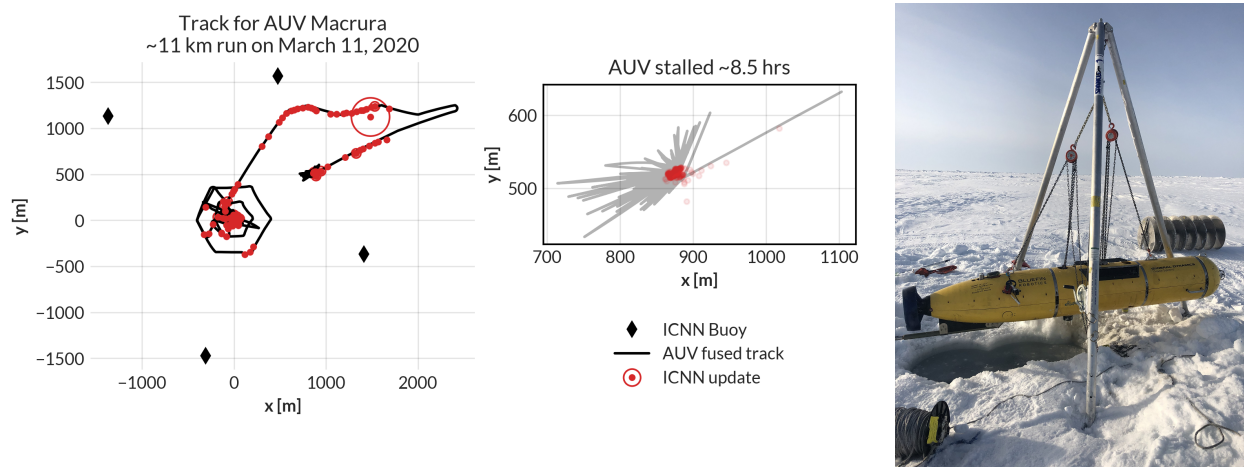


FIG. 2. The under-ice mission track for AUV *Macrura*, including the position updates as it stalled underneath the ice overnight. A marker was placed on the ice at the vehicle’s estimated self-location. It was recovered after a three day storm within a meter of the marker.

196 B. ICEX20 sound speed conditions

197 An important component to our navigation solution is an accurate estimation of a repre-
 198 sentative SSP for the ocean volume. Previous field experience, during the Ice Exercise 2016
 199 (ICEX16), demonstrated the negative effects of the Beaufort Lens on tracking and commu-
 200 nication (Schmidt and Schneider, 2016). Fig. 3 shows historical, modeled, and *in situ* sound
 201 speed data for both ICEX16 and ICEX20. These three input streams were selected to mirror

202 the information available on a submarine (personal conversation with LT B. Howard and LT
 203 CDR D. Goodwin). In the field, the SSP information was shared with the vehicle via basis
 204 representation compression on a lightweight digital acoustic message ([Bhatt et al., 2022](#)). All
 205 modeled data comes from HYCOM ([Chassignet et al., 2007](#)), which does not seem to capture
 206 the forcing mechanisms that cause the Beaufort Lens. For ICEX16, the data-driven profile
 207 was sourced from nearby Ice Tethered Profilers (ITP) after the field experiment ([Krishfield](#)
 208 *et al.*, 2008; [Toole et al., 2011](#)) and exhibits a fairly low lens; the historical profile is from
 209 the World Ocean Atlas. For ICEX20, the chosen weights (data-driven) profile derives from
 210 an estimate of initial CTD casts taken on site, showing an intense warm water intrusion; the
 211 baseline (historical) profile, showing moderate ducted conditions, comes from the average
 212 of March 2013 ITP data. This month best matched sea ice and sound speed conditions
 213 at the beginning of ICEX20 ([Bhatt et al., 2022](#)). It is important to note that all profiles
 214 that do show the Beaufort Lens do so with different local sound speed maxima at different
 215 depths, reflective of the wide range of lens properties observed for all ITP data in the region.
 216 The variability of the lens height and prominence is the main reason an updatable SSP was
 217 integrated into the ICNN solution.

218 During ICEX20, the HYCOM profile was available but never deployed. For post-
 219 processing comparison, we introduce both the HYCOM profile and an isovelocity case,
 220 1441.8 ± 3.7 m/s, as the mean and standard deviation of the observed sound speed profile
 221 over the first 200 m. This is a contrived value taken in the style of [Graupe et al. \(2019\)](#)
 222 for the sake of comparison; the default value in the LAMSS simulator, which was not
 223 environmentally informed nor used during ICEX20, was 1430 m/s.

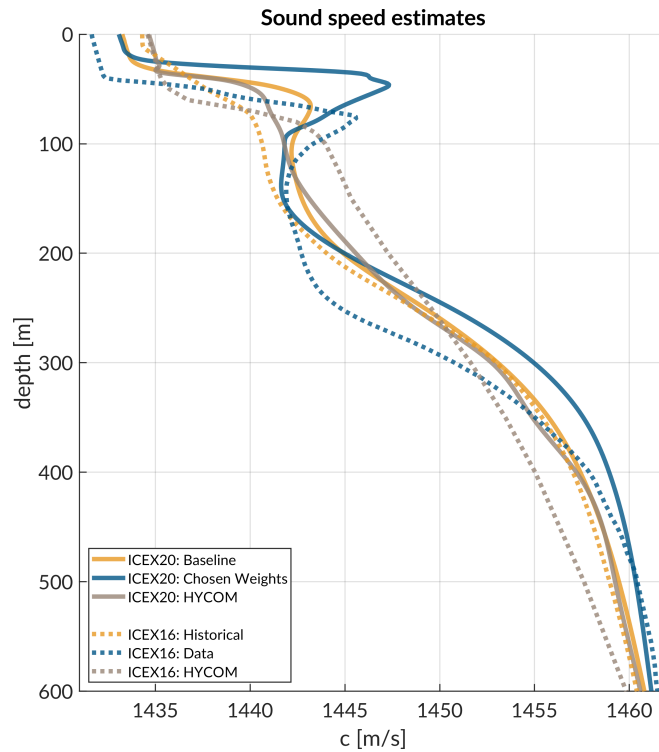


FIG. 3. Sound speed conditions for historical (baseline), data (chosen weights), and HYCOM model for both ICEX16 and ICEX20.

224 **III. REAL-TIME PSEUDORANGE ANALYSIS**

225 Because the vehicle’s navigation solution during a mission can only be evaluated on the
226 basis of the error estimates sent, a sister experiment for validating the real-time ranging
227 approach was implemented. Ice buoy modems were run as “virtual vehicles” at a fixed
228 depth, receiving position updates from the other beacons as well as a camp site modem
229 lowered to 20 m. Fig. 4 shows successful events sorted by source depth. In this analysis, we
230 assume there is insignificant displacement between the GNSS puck surface expression and
231 subsurface modem; this is supported by unusually low observed ice drift rates, just 0.7 cm/s
232 on average throughout the mission.

233 **A. Minimal bounce criteria (MBC)**

234 The fundamental challenge to implement GNSS-like navigation, especially in an acousti-
235 cally complex propagation environment, is characterizing a single sound speed to compensate
236 for the effects of ray refraction and reflection. The use of the acoustic modem network for
237 tracking relies on the accurate estimates of travel times between the submerged platform
238 and LBL beacons, supported by clock synchronization and a pre-determined scheduling of
239 acoustic events. For the Beaufort Lens in particular, the strong multipath effects make it
240 virtually impossible to deterministically predict the modem’s detected arrival time.

241 Instead, for each individual modem i , an embedded stochastic tracking framework is used
242 to provide a running estimate of the effective sound speed $c_{i,j}$ for the conversion from travel
243 time to range from modem j , with the ultimate goal of matching the implied horizontal

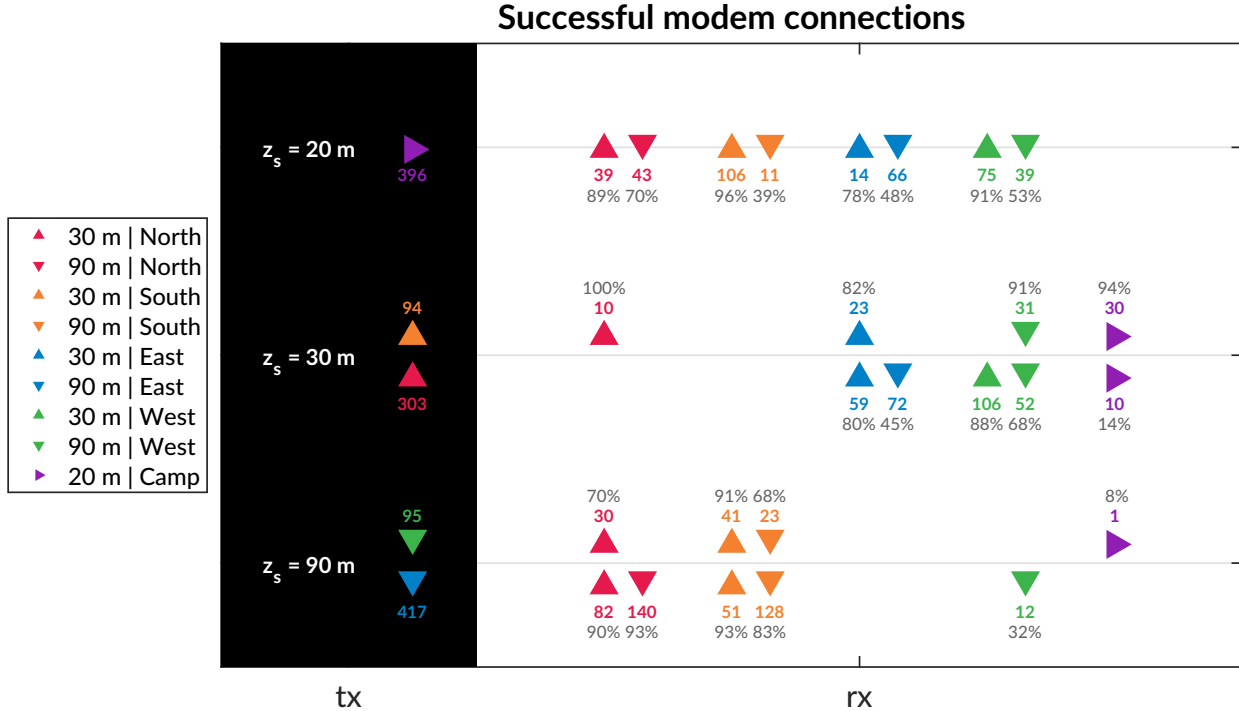


FIG. 4. An overview of the modem experiment by source and receiver depth and position. The black column on the left, *tx*, shows the source depth, z_s , with the total number of transmissions. The column on the right, *rx*, shows the receivers with the number of successful decodings and the percent success rate, defined as the ratio of decoded to detected. The orientation of the triangles—sideways, upwards, and downwards—corresponds to depths of 20, 30, and 90 m.

²⁴⁴ effective sound speed, i.e., the GPS-recorded distance between two nodes divided by the
²⁴⁵ modem-recorded one way travel time between them.

²⁴⁶ In the ICEX20 configuration, the acoustic tracking is running on the topside computer,
²⁴⁷ which controls the ICNN. Here we assume that the effective sound speeds $c_{i,j}$ are smoothly

²⁴⁸ varying over the course of a vehicle mission, i.e., with respect to range, mission time, and
²⁴⁹ the thirty-second frequency.

²⁵⁰ When the topside tracking framework receives a message, with a time delay, Δt , it will
²⁵¹ request a new estimate for $c_{i,j}$ along with its standard deviation. The effective sound speed
²⁵² is predicted using the vehicle's reported depth and the extrapolated navigation solution for
²⁵³ range, \hat{r} , as inputs to the ray tracing program, which returns an impulse response estimate
²⁵⁴ in the form of ray travel times dt_j and amplitudes a_j .

²⁵⁵ The initial call to BELLHOP is over a local grid centered at the range and depth posited
²⁵⁶ by the onboard tracking solution. The grid, compared to a point solver, adds redundancy
²⁵⁷ in resolving the actual multipath structure for a reliable acoustic path without overtaxing
²⁵⁸ onboard computational time and memory. It is initialized as 11×11 points spanning 10
²⁵⁹ m horizontally and 20 m vertically. The horizontal dimension reflects the accumulated
²⁶⁰ vehicle position error given a thirty-second communication cycle; the vertical dimension
²⁶¹ reflects how, computationally, eigenrays of the same timefront seem to stack vertically in
²⁶² the water column. For each grid point, BELLHOP produces a number of arrivals resulting
²⁶³ from multiple propagation paths. Using only the N_0 rays with neither surface nor bottom
²⁶⁴ bounces, it will then estimate the current effective sound speed c from a power weighted
²⁶⁵ average of the ray travel times,

$$c = \frac{\hat{r} \sum_{n=1}^{N_0} a_n^2}{\sum_{n=1}^{N_0} dt_n a_n^2}, \quad (1)$$

²⁶⁶ and the associated weighted standard deviation,

$$\sigma_c \simeq \sqrt{\frac{\sum_{n=1}^{N_0} (dt_n - \hat{r}/u)^2 a_n^2}{\sum_{n=1}^{N_0} a_n^2}} \frac{u^2}{\hat{r}} \quad (2)$$

²⁶⁷ If no direct paths exist, i.e. $N_0 = 0$, then the effective speed is computed using the same
²⁶⁸ algorithm for the ray arrivals with one bounce, and so on.

²⁶⁹ Finally, the pseudorange is calculated simply as

$$r_{i,j} = c_{i,j} \Delta t_{i,j} \quad (3)$$

²⁷⁰ Thus the MBC method assumes the signal detected by the modem will be dominated by
²⁷¹ a set of paths with the least number of boundary interactions. Importantly, this stochastic,
²⁷² ensemble method for group velocity calculation can run in real-time, appearing to be orders
²⁷³ of magnitude faster than other post-processing methods which seek to determine the specific
²⁷⁴ ray itself that best matches a prominent indicator from the arrival structure. The BELLHOP
²⁷⁵ simulation that runs this calculation uses 3600 rays with launch angle fan of -60 to 60 degrees,
²⁷⁶ a representative depth dependent sound speed profile, and a range dependent bathymetry.

²⁷⁷ B. Pseudorange error metrics

²⁷⁸ The sister modem experiment generated 811 beacon to beacon communication events with
²⁷⁹ their own real-time MBC group velocity predictions. Given the complexity of the ICNN
²⁸⁰ system, this experiment did not collect an exhaustive set of data across all buoy, source
²⁸¹ depth, receive depth, and sound speed combinations. The algorithm generally overestimates
²⁸² pseudoranges because it resolves the effective sound speed for the most direct path.

²⁸³ Fig. 5 shows the range error boundary for both SSP inputs used in ICEX20. A promising
²⁸⁴ sign that the MBC method adapts sound speed somewhat intelligently is the lack of error
²⁸⁵ growth as travel time increases. The baseline SSP ($n=243$ events) has an absolute pseudor-

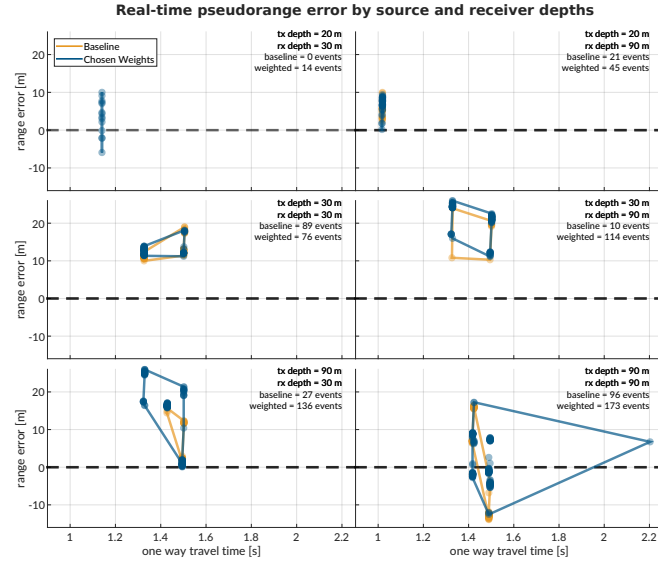


FIG. 5. The real-time range error by source (rows: 20, 30, and 90 m) and receiver (columns: 30 and 90 m) pairings for both sound speed estimates used during ICEX20. The amount of communication events is notated in the top right of each panel. The dashed line indicates no range error, and the boundary drawn indicates scope of the range error as a function of one way travel time.

286 range error of 11.38 ± 4.23 m; the weighted SSP ($n=568$), 11.36 ± 8.12 m. The discrepancy
 287 between these two is largely due to outlier events only contained in the weighted SSP set.
 288 Where there is overlap between sound speed conditions used for the real-time MBC, the
 289 pseudorange error difference is no more than a few meters. The overarching results show
 290 that sound speed estimates derived from eigenrays for a local grid, as opposed to a singular
 291 point, are accurate enough to support vehicle navigation. While the NBC looks for just the
 292 least complex multipath, the high density of launch angles almost always guarantees a direct
 293 path. Nonetheless, the consistent overestimation of pseudorange invites further analysis into
 294 acoustic arrival matching.

295 **C. Eigenray identification for beacon-to-beacon events**

296 Accounting for ice movement between beacons creates nominal ranges with small vari-
 297 ability. Figs. 6, 7, and 8 show eigenrays for three sound speed environments for source
 298 depths of 20, 30, and 90 m, respectively. Eigenrays were initially found using the built-in
 299 BELLHOP protocol with a launch angle fan of 2400 rays between -60 and 60 degrees. Sepa-
 300 rately, recorded travel times between beacons were clustered with 1 millisecond boundaries
 301 such that some source-receiver pairs had multiple, distinct travel times to approximate. The
 302 BELLHOP eigenray returns were then filtered such that one was selected per travel time
 303 cluster, in the hopes that the eigenray will converge to the receiver locations for the most
 304 realistic sound speed input. It should be noted that bottom bounces were recovered but
 305 filtered out. The three source depths create distinct ray geometries with respect to the three
 306 sound speed inputs.

307 **1. Source depth of 20 m**

308 For a source at 20 m in depth, shown in Fig. 6, reliable eigenrays are found for all sound
 309 speed inputs. Rays refract upwards and neatly intersect with the shallow and deep receiver
 310 locations between 1.5 and 1.8 km in range. However, the ray paths for the shallow receivers
 311 change both in the number of surface interactions and where the surface interactions occur
 312 with respect to range across the SSPs. As the Beaufort Lens strengthens, the chosen paths to
 313 the second farthest shallow buoy (North, in red) interact with the surface more and become
 314 distinct. The weighted SSP shows the most interesting effects for the deeper receivers. The

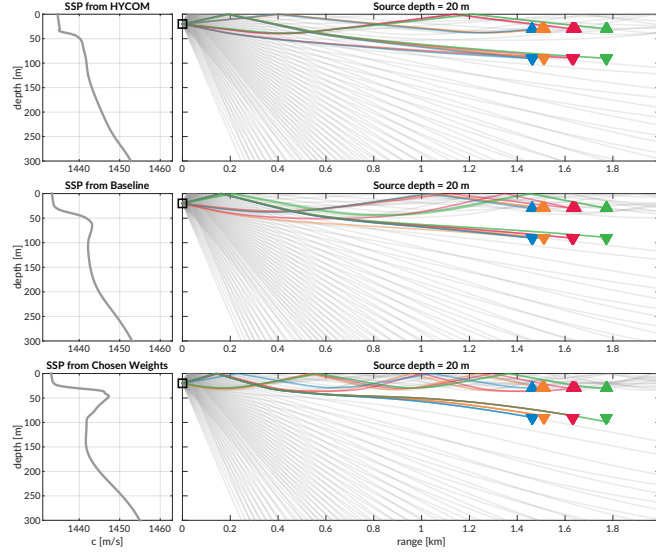


FIG. 6. Eigenrays for beacon-to-beacon events for each sound speed with a nominal source depth of 20 m over a total ray fan in gray. The beacons are highlighted in color/marker coding in Fig. 4.

315 ray paths all interact with the surface and the eigenrays for the Northern (red) and Western
316 (green) buoys are in fact the same ray.

317 **2. Source depth of 30 m**

318 The ray geometries from the 30 m source, shown in Fig. 6, show a similar degradation
319 of eigenray identification with increased ducting. Receptions span 1.5 to 3.2 km. Once
320 again, eigenrays for HYCOM and the baseline SSP are visually appropriate. Rays for the
321 weighted SSP show how the surface channel intensifies ice interactions and how the shadow
322 zone denies reliable acoustic paths. Pointedly, the increasing number of surface reflections to
323 the farthest shallow buoy (North, in red) crystallize the MBC's tendency for overestimation.
324 For the HYCOM, baseline, and weighted SSP inputs, the most appropriate eigenrays show
325 2, 3, and 4 surface interactions.

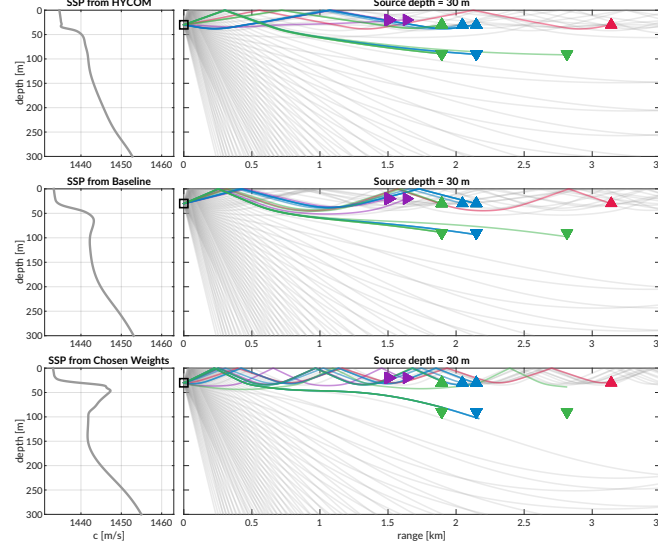


FIG. 7. Eigenrays for beacon-to-beacon events for each sound speed with a nominal source depth of 30 m over a total ray fan in gray. The beacons are highlighted in color/marker coding in Fig. 4.

326 **3. Source depth of 90 m**

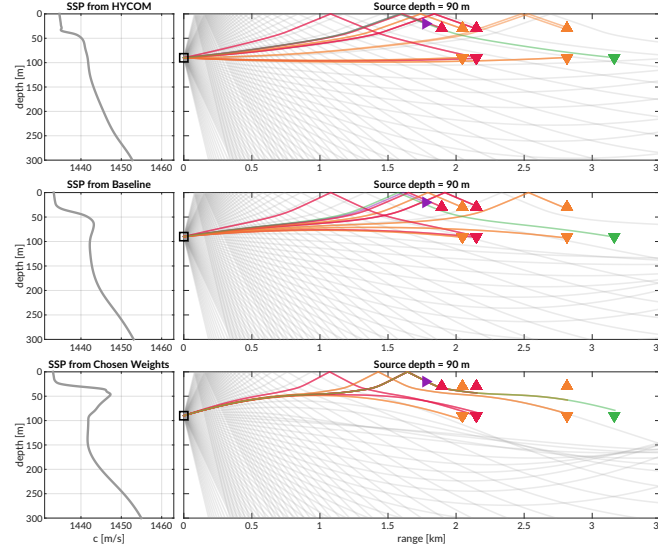


FIG. 8. Eigenrays for beacon-to-beacon events for each sound speed with a nominal source depth of 90 m over a total ray fan in gray. The beacons are highlighted in color/marker coding in Fig. 4.

327 Lastly, Fig. 8 shows ray geometries from the 90 m source, elucidating a different extent
328 of the shadow zone. While the receiver locations are similar to that of the 30 m source
329 depth, the deeper source depth effectively negates the upper duct and places the upper (and
330 some of the lower) receivers in unreliable acoustic paths. The HYCOM eigenrays still show
331 the most reliable acoustic paths that deteriorate with increasing ducted conditions. The
332 lack of direct paths from the observed SSP further points out the shortcomings of the MBC
333 approach.

334 The goal of the MBC algorithm was to provide a reliable, physically intuitive interpre-
335 tation of the acoustic propagation without taking on the additional burden of regularly
336 identifying specific paths that may connect any given source-receiver pair in the network.
337 While it was unlikely to resolve multipath arrivals that triggered successful modem detec-
338 tion, an isovelocity approach would have provided no adaptivity against source and receiver
339 depth differences. Its performance was adequate for vehicle navigation and would have likely
340 sufficed if it were not for the prominence of the duct observed relative that of other model
341 and data products.

³⁴² **IV. POST-PROCESSED PSEUDORANGE ANALYSIS**

³⁴³ From all events recorded during the modem test experiment, there are 1242 successfully
³⁴⁴ decoded beacon-to-beacon events. Thus, a post-processing analysis that emulates the real-
³⁴⁵ time navigation engine was run to overcome the unequal distribution of communication
³⁴⁶ events with respect to depth, range, and sound speed status.

³⁴⁷ It is important to note that the value for the extrapolated range, \hat{r} , is only tracked when
³⁴⁸ the modem runs the vehicle behavior; thus we replace \hat{r} with the GPS-tracked range for
³⁴⁹ all modem events. Because \hat{r} converges to the correct solution, a comparison of \hat{r} with the
³⁵⁰ GPS-tracked range shows a normal, zero-centered distribution within the bounds of GPS
³⁵¹ drift. The analysis therefore seeds realistic but “omniscient” knowledge of the extrapolated
³⁵² range and emulates the post-processing pipeline to more thoroughly evaluate the acoustic
³⁵³ pseudorange estimate for all modem events. Sound speed inputs are the isovelocity sound
³⁵⁴ speed in addition to the modeled, baseline, and weighted SSPs from Fig. 3. The analysis
³⁵⁵ replicates the MBC but also introduces a new filtering algorithm, the nearest bounce criteria
³⁵⁶ (NBC), based on insights gleaned from the eigenray analysis. Accordingly, the results in
³⁵⁷ this section evaluate the utility of the algorithms and sound speed sources, divorced from
³⁵⁸ their role in the ICNN while maintaining real-time relevance.

³⁵⁹ **A. Nearest bounce criteria (NBC)**

³⁶⁰ The extent of ray bending and repeated reflections is extremely dependent on the degree
³⁶¹ of the Beaufort Lens observed. Based on this insight, a new algorithm, the nearest bounce

³⁶² criteria (NBC), is a slight modification from the MBC and includes multipath as a new
³⁶³ dimension of information to exploit. This metric, while run in post-processing, adds a
³⁶⁴ negligible amount of computation for real-time efficacy.

³⁶⁵ Given a running estimate for the effective sound speed $c_{i,j}$ between nodes i and j , the
³⁶⁶ navigation system has an extrapolated value for range, \hat{r} , and a recorded travel time, $\Delta t_{i,j}$.
³⁶⁷ Instead of using only the N_0 rays with neither surface nor bottom bounces to estimate
³⁶⁸ conversion speed, and subsequently moving to incremental number of bounces only when no
³⁶⁹ valid direct path solutions exist, we solve for the power weighted average of the ray travel
³⁷⁰ time for the N_k rays with k bounces,

$$t_k = \frac{\sum_{n=1}^{N_k} dt_n a_n^2}{\sum_{n=1}^{N_k} a_n^2}, \quad (4)$$

³⁷¹ find the nearest matching power weighted average to recorded travel time,

$$t_{i,j,k} = \min_{k=0,1,2,\dots} |t_k - \Delta t_{i,j}| \quad (5)$$

³⁷² predict an effective sound speed,

$$c_{i,j} = \frac{\hat{r}}{t_{i,j,k}} \quad (6)$$

³⁷³ and estimate the range as was done previously.

$$r_{i,j} = c_{i,j} \Delta t_{i,j} \quad (7)$$

³⁷⁴ This method selects a different effective sound speed based on the multipath arrival struc-
³⁷⁵ ture, as the detected arrival is not always the first arrival or the direct path and could even
³⁷⁶ be masked by noise or blocked temporarily (Deffenbaugh *et al.*, 1996b). We manually cap

³⁷⁷ the number of bounces at four because of the smaller operational scale and the attenua-
³⁷⁸ tion accrued with many surface interactions. Bottom bounces are not encoded separately
³⁷⁹ because of ray's tendency to refract upward, not due to information limitations.

³⁸⁰ **B. Effective sound speed predictions**

³⁸¹ The minimal and nearest bounce algorithms are applied with the three sound speed inputs
³⁸² shown in Figs. 6, 7, 8. The resulting predicted effective sound speeds are shown in Fig. 9
³⁸³ for all source depths versus one way travel time.

³⁸⁴ The goal of the effective sound speed prediction is to converge towards the implied sound
³⁸⁵ speed, i.e. the GNSS-derived range divided by the recorded travel time. As the environ-
³⁸⁶ mental and ray filtering method become better representations of the real ocean, the lower
³⁸⁷ the expected mismatch is between the implied and estimated effective sound speeds.

³⁸⁸ The various sound speed inputs—isovelocity aside—not only modify the predicted effec-
³⁸⁹ tive sound speed, as seen by the colored vertical offsets, but often classify a distinct number
³⁹⁰ of bounces. HYCOM sees the most direct and one bounce multipath structures, lending a
³⁹¹ bias for faster speeds; the weighted SSP sees the most double and triple bounces, favoring
³⁹² slower speeds; the baseline sound speed exists in between. Very rarely is the multipath
³⁹³ structure classified as a direct path, where the MBC and NBC would prediction overlap. In
³⁹⁴ fact, the higher the multipath classification, the more accurate the sound speed prediction
³⁹⁵ is, likely driven by a tighter or even sparser bundle of rays. Discontinuities in multipath
³⁹⁶ classification provide initial evidence for its importance to a smoothly varying group veloc-
³⁹⁷ ity, as shown in the cluster of 30 to 30 m transmissions, where HYCOM jumps from one to

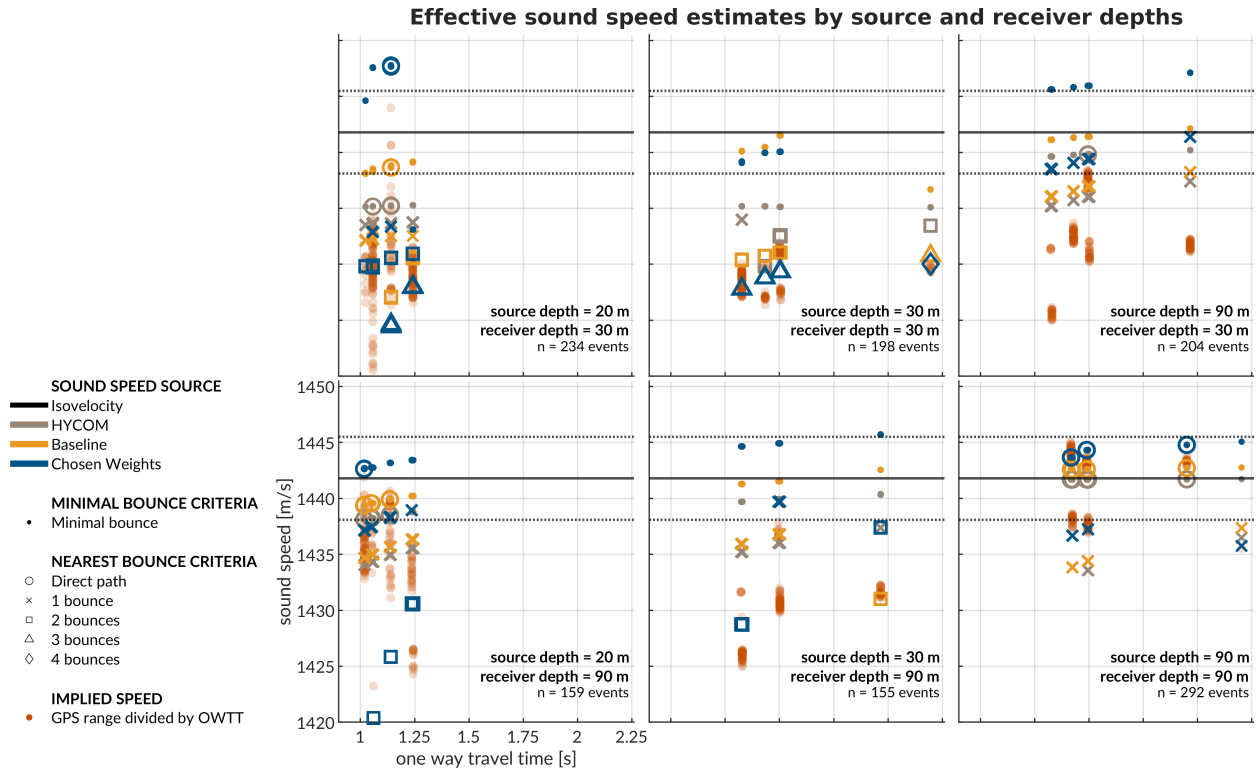


FIG. 9. A post-processing comparison of effective sound speed predictions for all beacon-to-beacon events. The rows share receiver depth; the columns share source depth. The recorded travel time is on the x-axis and the predicted effective sound speed is on the y-axis. The sound speed source is indicated by color. The isovelocity is shown as the mean \pm the standard deviation. The minimal and nearest bounce criterion are distinguished by different marker shapes, compared to the separately colored red dots showing the implied calculation.

398 two classified bounces amidst the baseline SSP and weighted SSP smoothly increasing while
 399 consistently seeing two and three classified bounces, respectively. Of course, the prediction
 400 deteriorates with cross-layer transmissions across the duct, but not to the same degree at
 401 which eigenrays could not be found for the weighted SSP in section III C. The evidence sug-

⁴⁰² gests that the grid based method provides a useful amount of redundancy to resolve similar
⁴⁰³ enough eigenrays.

⁴⁰⁴ It is useful to think about in what case the isovelocit—or any isovelocit framing—would
⁴⁰⁵ have been appropriate. The transmissions from shallow to shallow receiver would may have
⁴⁰⁶ matched the default configuration of 1430 m/s. The isovelocit contrived for this paper,
⁴⁰⁷ 1441.8 m/s, best matches the transmissions from 90 to 90 m. The one from [Graupe *et al.*](#)
⁴⁰⁸ ([2019](#)), 1450 m/s, would have had a systemic overestimation. Given that implied sound
⁴⁰⁹ speeds just for beacon-to-beacon events span 1420 to 1445 m/s, it is safe to say that a
⁴¹⁰ nominal sound speed would sacrifice pseudorange accuracy somewhere, and that an adaptive
⁴¹¹ approach is necessary even for short range operations in the Beaufort Lens.

⁴¹² C. Pseudorange error metrics

⁴¹³ Pseudorange estimation plays an important role in trilateration. Fig. [10](#) shows the
⁴¹⁴ directional pseudorange error “footprints” for the four sound speed inputs with the NBC
⁴¹⁵ approach, separated by source and receiver depth configurations.

⁴¹⁶ The weighted SSP range error generally has the smallest and most zero-centered footprint.
⁴¹⁷ The one case it does not is for the source-receiver pairings between 30 and 90 m in depth. The
⁴¹⁸ increased error for these is most likely driven by the computational artifacts encountered
⁴¹⁹ when propagating through the steep sound speed gradients of the lens and through the
⁴²⁰ shadow zone. All other source depth pairings are significantly improved using the chosen
⁴²¹ weights compared to HYCOM or the baseline.

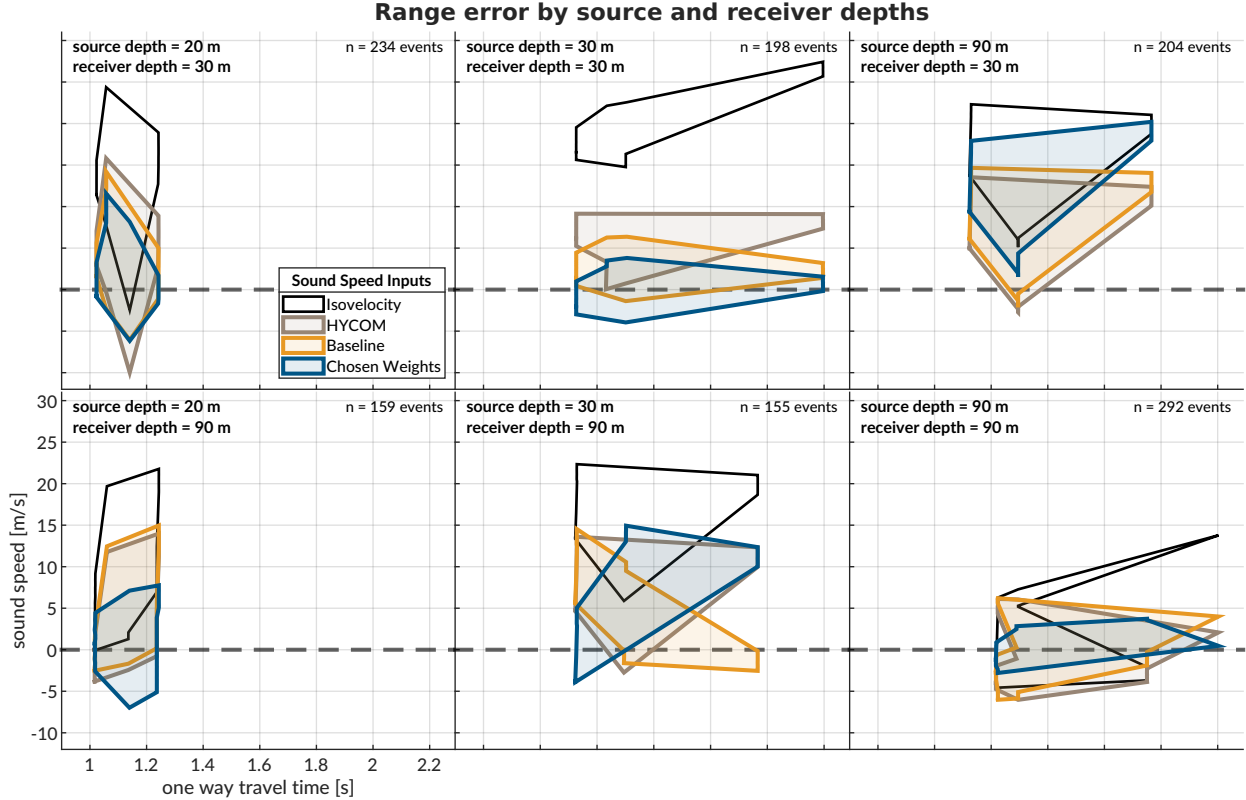


FIG. 10. The post-processed pseudorange error; the rows share receiver depth; the columns share source depth. The dashed gray line shows no error. The shaded region connects the range performance across all events.

When using a linear scaling to convert travel time into range, any offset between the assumed sound speed and the horizontal group velocity produces unconstrained error with increasing receiver distance, whereas an adaptive estimate would exhibit no such trend. This is easily observed in the same-layer links, i.e., 30 to 30 m and 90 to 90 m. In cross-layer links, the isovelocity does not perform better but tends to exaggerate or flip the footprint created adaptively.

The improvement from MBC to NBC is most evident for the data-driven sound speed; while the HYCOM SSP improves from a median absolute range error of 6.41 to 4.61 m,

430 the baseline SSP improves from 10.30 to 2.27 m, and the weighted SSP improves from
431 13.28 to 2.12 m. In comparison, the isovelocity has a median error of 13.09 m. The order
432 of magnitude improvement in the ducted SSPs demonstrate the effectiveness of the NBC
433 algorithm exploiting the observed multipath conditions.

434 There is one example that helpfully illustrates the improvement brought upon by bounce
435 classification. For transmissions between North and South at 30 m, the OWTT spread is
436 2.1958 to 2.1963 s; the GNSS-tracked distance is 3138.54 to 3140.87 m; and the implied
437 effective sound speed is 1429.3 to 1430.1 m/s. For these transmissions, the weighted SSP
438 and the MBC approach produce a pseudorange error of -1491 m, as the effective sound speed
439 is dominated by bottom bounce arrivals with much greater travel times. The NBC approach
440 categorizes this same record as a quadruple surface bounce, reducing the pseudorange error
441 to less than a meter. Comparatively, the NBC approach for HYCOM and the baseline
442 SSP produce pseudorange errors of 8.30 and 2.39 m, respectively. There is strong evidence
443 to suggest that the sound speed and multipath fidelity codependently improve localization
444 accuracy.

445 V. TRILATERATION FOR ICEX20 FIELD DATA

446 To overcome potentially intermittent acoustic communication, the operational paradigm
 447 of the ICNN computes corrections relative to the trilaterated position estimates transmitted
 448 by the vehicle, rather than transmitting the updated positions themselves. The reliability of
 449 the correction is directly linked to how accurately the travel time measurements are converted
 450 to pseudoranges. This section aims to resolve that tension by reevaluating the trilateration
 451 results with respect to the MBC and NBC algorithms. The MBC/NBC effective speed
 452 predictions were tracked independently for each source-receiver pair; although the sound
 453 speed was expected to be locally smooth near a given receiver, no such assumption was
 454 enforced between distinct acoustic links.

455 A. Re-positioning beacon to beacon events

456 When the beacons ran as virtual vehicles, the ICNN did not have access to that buoy's
 457 GPS data stream except for what was sent via digital acoustic message. The static nature of
 458 the experiment means that the initial estimate transmitted to the ICNN was in fact a ground
 459 truth position. Therefore, a distribution of corrections from the ICNN, as shown in Fig. 11,
 460 reflects positioning accuracy. The NBC clearly outperforms the MBC, with almost 80% of
 461 the corrections below 6 meters and the median within the deployed GNSS puck precision
 462 of 3 meters. By contrast, the MBC shows roughly 20% within the GNSS puck precision,
 463 and separate peaks from 9–12 meters and 21–27 meters. This trimodal nature reflects the
 464 distribution of reflections on the ice surface.

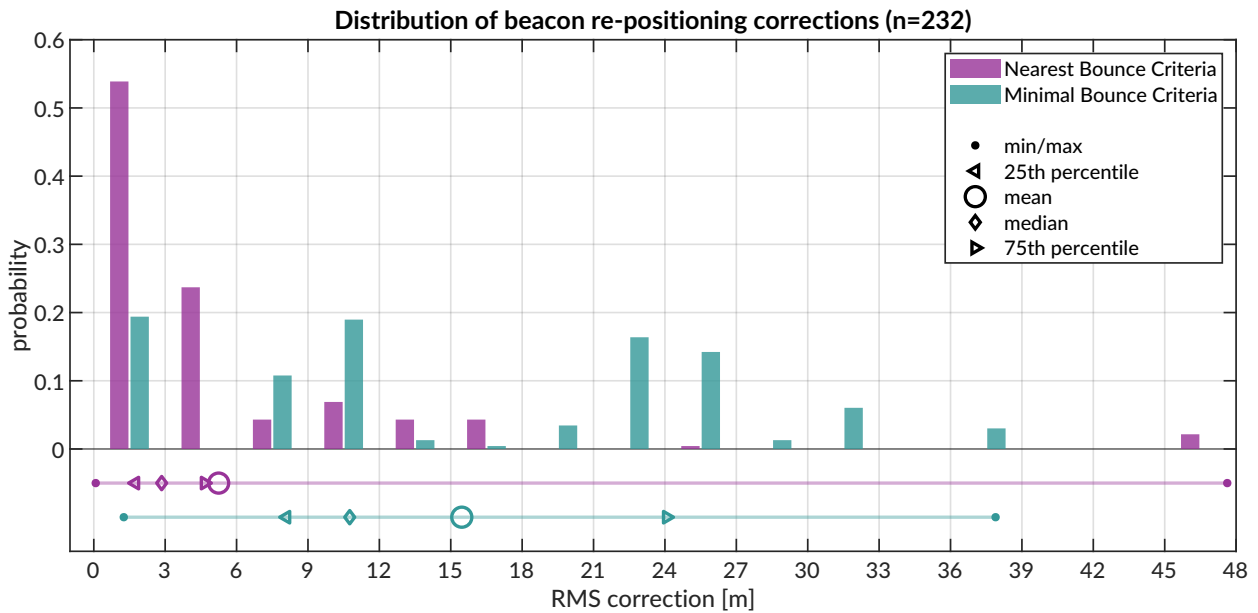


FIG. 11. Trilateration events; however, 264 entries are 2-beacon solutions, 22 are 3-beacon, and 2 are 4-beacon. When limited to only two ranging circles, the trilateration chooses the closer of the two intersection points. The x-axis is cut off at the upper limit for the NBC algorithm.

465 In several events, the MBC is unable to accurately estimate the effective sound speed for
 466 one of the acoustic links, leading to a large positioning error. The NBC, however, better
 467 resolves an approximation of the acoustic path. For example, in some trilateration solutions
 468 for the Eastern buoy, the MBC shows a correction of more than a kilometer; the NBC is
 469 two orders of magnitudes less.

470 **B. Re-navigating AUV *Macrura***

471 Up to this point, pseudorange estimation and localization have been evaluated on GPS-
 472 linked beacon-to-beacon connections to validate the NBC algorithm. This analysis ports the
 473 MBC and NBC algorithms to re-navigate the AUV *Macrura*.

474 In comparison to the modem experiment, the AUV data clearly exhibit instances where
 475 a receiver detects the same transmission more than once. This is not surprising considering
 476 the complex multipath provided by the Beaufort Lens. The 11 hour vehicle mission con-
 477 tains 3,260 transmissions, 12,938 total detections, and 4,704 successful receptions. Allowing
 478 receptions with PSK errors would almost double the number of recorded multipath arrivals
 479 exploited for positioning, if a real-time solution could correctly parse paths from different
 480 arrivals in the same thirty-second cycle. Thus it remains a future endeavor to explore how
 481 failure mode information from acoustic modems could be used to identify unsuccessful but
 482 otherwise trustworthy arrivals to augment trilateration samples.

483 The following performance analysis is constrained to what the vehicle acted on in real-
 484 time. AUV *Macrura* and the ICNN ran an adaptive depth behavior to maintain acoustic
 485 communication on the insight that cross-layer links were more likely to fail than same-layer
 486 ones. Accordingly, the vehicle dove deeper than 50 meters about 20% of the time it was
 487 underway.

488 In contrast to the modem tests, where position correction illustrated re-positioning ac-
 489 curacy, the re-navigation corrections are less valuable in the absence of GNSS ground truth.
 490 The correction magnitude necessarily depends on the vehicle's internal navigation estimate,
 491 which is prone to larger errors from sensor drifts, ocean currents, and other error not cap-
 492 tured in the hydrodynamic model. Thus, larger corrections are not necessarily indicative of
 493 worse performance. Navigation accuracy is better described by trilateration error, the RMS
 494 of the remaining pseudorange errors from each acoustic link.

495 Fig. 12 shows the correction magnitudes and trilateration errors for events with three or
 496 more receptions during AUV operations. Whereas the MBC has a fairly bimodal nature,
 497 with peaks centered around 10–15 and 35–40 m, the NBC favors smaller corrections, from
 498 5–20 m, and has a long tail. The distribution of corrections are much larger than the
 499 distribution of RMS error. It is apparent that, while both methods are quite successful,
 500 there is strong evidence that the NBC achieves single meter accuracy.

501 C. Investigating potential GNSS noise

502 The fact that the bulk of the best performing re-navigation error exists within the pre-
 503 cision of the GNSS unit deployed invites a further look into GNSS noise. In the Arctic,
 504 GNSS performance worsens due to poor constellation coverage, larger ionospheric effects,
 505 and multipath interference. The National Security Implications of Climate Change for U.S.
 506 Naval Forces (Council, 2011) details some of the limitations of the Global Positioning Sys-
 507 tem (GPS) at polar latitudes. Radio infrastructure that provides position corrections and
 508 references does not regularly extend to polar regions. The effect is minor for surface plat-
 509 form navigation —roughly 15 m of horizontal precision has been displayed at the North
 510 Pole—but is significant enough to register against the modem’s detected travel times. Fig.
 511 13 zooms in on the GNSS and OWTT noise relative to the ice movement for two pairs of
 512 modem buoy connections. The two panels indicate the GPS drift as $\delta R = \sqrt{\delta x^2 + \delta y^2}$ and
 513 temporal drift, δt , relative to the median OWTT recorded between the two modems. The
 514 dashed line is scaled by a group velocity of 1440 m/s, such that if there were ideal sensor
 515 measurements with no drift, all events should exist on or near the line.

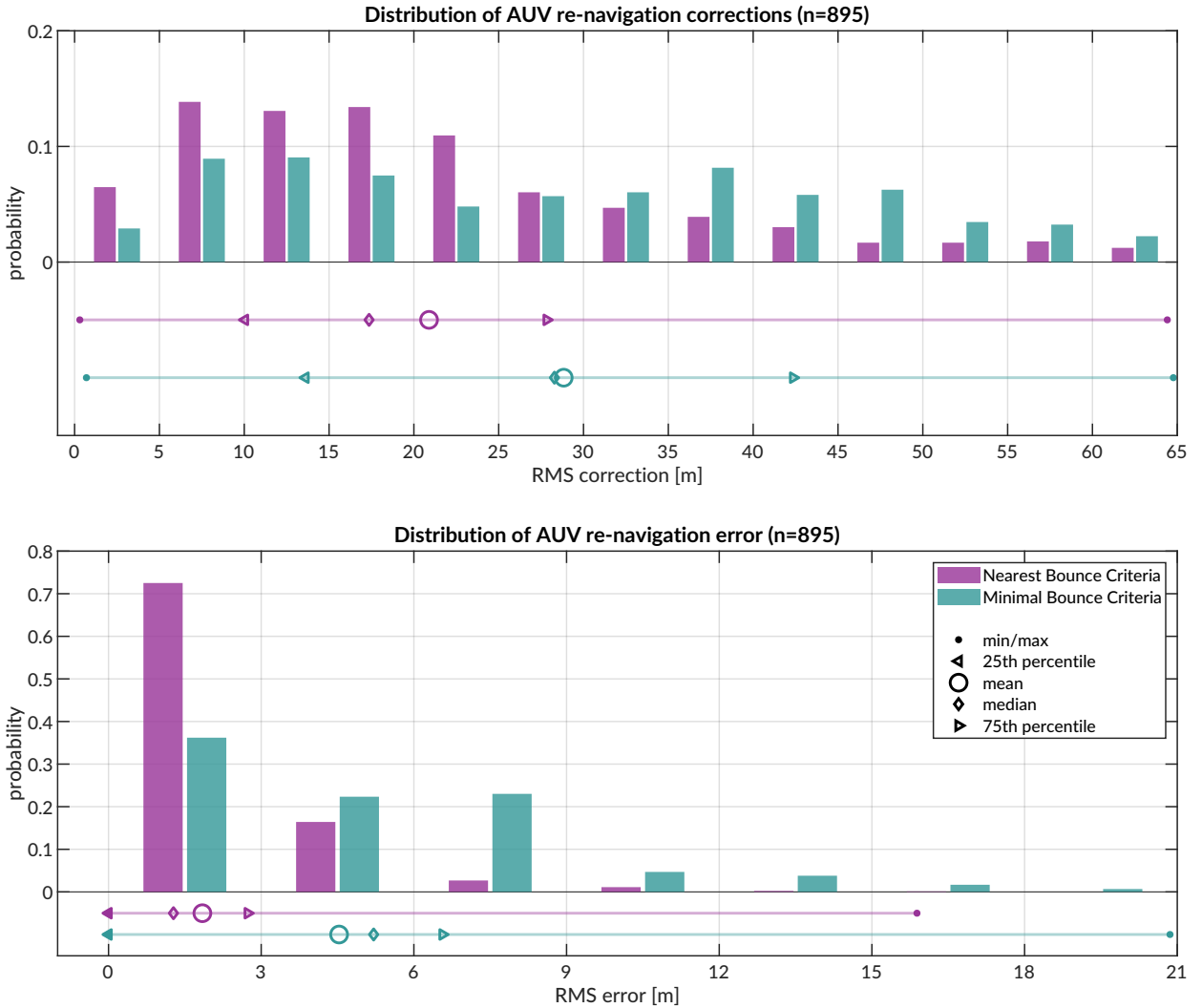


FIG. 12. Distribution of vehicle re-navigation corrections (top) and error (bottom) computed in post-processing for the Minimum and Nearest Bounce Criterion.

516 The top panel shows the connections between the North and East buoys. The clusters
 517 scaling along the 1440 m/s guideline suggest relative ice movement picked up by both GNSS
 518 and OWTT. But the vertical distribution across many arrival time bands is indicative of
 519 the GNSS fluctuations in precision, or noise. Some minor offsets between these vertical
 520 bands relate to different operational configurations of source and receiver depth. The idea

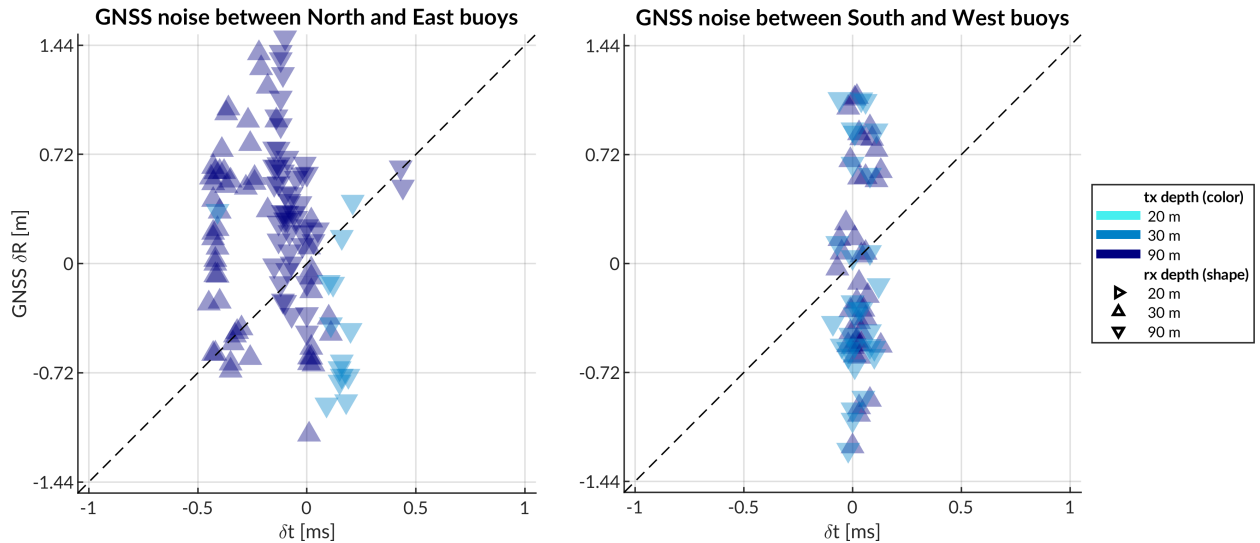


FIG. 13. A comparison of GPS drift (y-axis) versus OWTT drift (x-axis), colored by source and receiver depth.

of GNSS noise relative to OWTT is further indicated by events between two other buoys, South and West. The relatively thin time window suggests these buoys are moving in a more rigid ice floe and that there is minimal impact by source and receiver depth on the spread of OWTT. Yet, the vertical distribution, spanning almost 4 meters, cannot be explained by time differentials due to acoustic scattering, multipath, and/or environmental microstructure.

VI. DISCUSSION

Given the computational constraints of real-time modeling, the gridded approach facilitates enough multipath classification to build in a “ray ensemble” of characteristic group velocities. This result is not always possible when aiming to find eigenrays to just an individual point, even with a higher density of launch angles. An important takeaway for those

532 interested in ray-based localization is leveraging a local grid to give BELLHOP tolerance
533 for finding solutions that otherwise may not be found in a center or single point solution.
534 The limitations of numerical computation, particularly for a complex environment, are more
535 adeptly addressed by accepting some uncertainty in position than by prescribing an exact
536 solution. Even though BELLHOP is a greedy estimator for eigenrays, the additional data
537 created is a negligible burden.

538 Underwater navigation research is broadly motivated by acquiring GPS-like navigation
539 accuracy in GPS-denied conditions. The Arctic, while remote, is the perfect place to test
540 mature navigation technologies in real GPS-denied conditions.

541 Range estimation is an essential step of acoustic localization and navigation. Current
542 approaches in real-time underwater acoustic navigation simplify the non-linear relationship
543 between a sound speed profile and acoustic propagation with a deterministic sound speed.
544 Some post-processing approaches attempt to leverage the acoustic arrival structure via var-
545 ious ray methods, but often use a singular SSP for simplicity, even over long term missions
546 or dynamic conditions. Thus, the conversion from travel time to range, particularly for
547 real-time vehicle deployments, can be pre-conditioned for error growth as the OWTT/range
548 increases.

549 For GPS-denied navigation, especially in hostile environments like the Arctic, tolerance
550 for error is close to none. This work addresses a critical need in acoustic navigation by
551 retooling acoustic arrival methods generally deemed too complex or labor intensive for real-
552 time, ray-based range estimation to achieve GPS-like positioning.

553 We hypothesize and validate that the embedded stochastic prediction of a single group
 554 velocity is a smoothly varying function of range, source and receiver depth pairings, as
 555 well as multipath structure. We employ a GPS-tracked experiment to have a ground truth
 556 comparison for real-time localization algorithms. The real-time system achieves GPS-like
 557 navigation for an AUV without taking into account multipath structure; the ranging error
 558 improves by an order of magnitude with the suggested multipath adaptability, minimizing
 559 range error to single meters. Post-processing analysis shows that this method of ranging is
 560 sensitive to GPS drift itself; thus embedding a stochastic prediction of the horizontal group
 561 velocity has an outsized benefit to minimizing trilateration error.

562 There are many avenues through which this approach can be further refined and tested for
 563 field operations. Amongst them is defining the uncertainty grid for BELLHOP via stochastic
 564 or data-driven measures such as the distance traveled by the AUV between ICNN updates
 565 or the magnitude of the position corrections by the ICNN. Another is to entirely remove the
 566 seeded range and instead rely on the submerged asset's depth and recorded OWTT to find
 567 high probability fields in range.

568 The literature in underwater acoustic navigation and positioning is either real-time or
 569 physics-based. In this paper we demonstrate a field-tested approach that is both real-time
 570 and physics-based; this is achieved by coupling data streams with fast acoustic modeling.
 571 The methods exploit the upward refracting nature and the total ice cover of the Arctic
 572 environment to achieve remarkable ranging accuracy and precision. It transforms multipath,
 573 widely considered as an obstacle for acoustic ranging, into a new information content to
 574 refine ranging accuracy. We believe that this work enables more accurate range estimation,

575 localization, and/or navigation for any field experiment given known source and receiver
576 depths.

577 Performance in other acoustic environments may require introducing a different thresh-
578 olded metric to sort time of arrivals. Given the NBC algorithm's improvement with increased
579 multipath, its effectiveness is likely only challenged by the valid operational scales of a range
580 independent propagation environment. For mesoscale operations, like that of many glid-
581 ers, the group velocity criteria may need to be modified to better account for variability
582 driven by range dependent propagation through internal waves, eddies, or even bathymetric
583 changes like underwater volcanoes. BELLHOP simulations provide other relevant eigenray
584 information, like time and angle of arrival, that is ripe for statistical and machine learning
585 methods to classify a representative group velocity. A bespoke and fast ray tracing method,
586 which was used during ICEX20 to evaluate the acoustic fit of sound speed profile parame-
587 terization ([Bhatt et al., 2022](#)), can easily report back the number of turning points instead
588 of the number of bounces for multipath classification.

589 This approach will start to break down in extremely dynamic environments, like fast
590 moving fronts. Realistic *in situ* considerations of the acoustic environment may not be pos-
591 sible without complete through-the-sensor integration of acoustic dat and/or hyper realistic
592 ocean models.

593 Many approaches to underwater navigation combine it with acoustic tomography, i.e.,
594 a joint estimation of both source and receiver locations and the ocean volume between
595 them. There has been considerable success at this effort in post-processing methods,
596 which utilize intensive—and due to the non-linearity of sound propagation, often brute

597 force—computational methods. For vehicle operations, fast tomography is the ideal im-
598 plementation, in that one can fully consider how sound speed structure, horizontally and
599 vertically, influences sound propagation. AUVs can serve as moving sources to better image
600 the ocean volume (Deffenbaugh, 1997; Elisseeff *et al.*, 2002), where mobile tomography and
601 navigation converge on the same set of component technologies: position estimation, sound
602 speed parameterization estimation, ray path identification, and vehicle path optimization.

603 But there are overwhelming challenges, operationally and computationally, for fast, mo-
604 bile tomography to become a realistic endeavor. Addressing the spatial and temporal scales
605 of what can be solved deterministically and what must be solved stochastically imposes a
606 resolution constraint on the utility of gridded models—resolving fine features inaccurately
607 (or with a false sense of confidence) could be more harmful than assuming range indepen-
608 dence. Given that AUV operations are often on small spatial and temporal scales, the added
609 benefit of a gridded model is quite small, and in cases like the Arctic, may actually mis-
610 characterize the ocean volume. For gliders, with longer and larger operational scales, an
611 ocean model may provide more useful information. Currently gliders are low power and do
612 not have the storage or computational power to run a full-scale, realistic ocean model. A
613 lightweight representation of the key environmental and acoustic features, passed through
614 the same manner of acoustic message from the modem experiment, may drastically improve
615 glider navigation.

616 **ACKNOWLEDGMENTS**

617 We acknowledge the significant operational effort spearheaded by the LAMSS ICEX20
 618 team and all our collaborators. Bhatt was funded by a National Defense, Science, and
 619 Engineering Graduate Fellowship. This work was supported by the Office of Naval Research
 620 322-OA under ICEX20 (N00014-17-1-2474) and Task Force Ocean (N00014-19-1-2716).

621

622 Ballard, M. S., Badiey, M., Sagers, J. D., Colosi, J. A., Turgut, A., Pecknold, S., Lin, Y.-T.,
 623 Proshutinsky, A., Krishfield, R., Worcester, P. F., and Dzieciuch, M. A. (**2020**). “Tem-
 624 poral and spatial dependence of a yearlong record of sound propagation from the Canada
 625 Basin to the Chukchi Shelf,” The Journal of the Acoustical Society of America **148**(3),
 626 1663–1680, <http://asa.scitation.org/doi/10.1121/10.0001970http://files/814/>
 627 [Ballardetal.-2020-Temporalandspatialdependenceofayearlongreco.pdf](#), doi: [10.1121/10.0001970](https://doi.org/10.1121/10.0001970).

628 Barker, L. D. L., Jakuba, M. V., Bowen, A. D., German, C. R., Maksym, T., Mayer,
 629 L., Boetius, A., Dutrieux, P., and Whitcomb, L. L. (**2020**). “Scientific challenges and
 630 present capabilities in underwater robotic vehicle design and navigation for oceanographic
 631 exploration under-ice,” Remote Sensing **12**(16), 1–31, doi: [10.3390/RS12162588](https://doi.org/10.3390/RS12162588).

632 Bellingham, J., Leonard, J., Vaganay, J., Goudey, C., Atwood, D., Consi, T., Bales, J.,
 633 Schmidt, H., and Chryssostomidis, C. (**1995**). “Auv operations in the arctic,” in *Sea Ice*
 634 *Mechanics and Arctic Modeling Workshop*.

- 636 Bhatt, E. C. (2021). “A Virtual Ocean framework for environmentally adaptive, em-
 637 bedded acoustic navigation on autonomous underwater vehicles,” Ph.D. thesis, Mas-
 638 sachusetts Institute of Technology and Woods Hole Oceanographic Institution Joint Pro-
 639 gram, <https://hdl.handle.net/1912/27309>, doi: [10.1575/1912/27309](https://doi.org/10.1575/1912/27309).
- 640 Bhatt, E. C., Howard, B., and Schmidt, H. (2022). “An Embedded Tactical Decision Aid
 641 Framework for Environmentally Adaptive Autonomous Underwater Vehicle Communica-
 642 tion and Navigation,” IEEE Journal of Oceanic Engineering .
- 643 Brooke, J. (1981). “Arcs (autonomous remotely controlled submersible),” in *Proceedings of*
 644 *the 1981 2nd International Symposium on Unmanned Untethered Submersible Technology*,
 645 IEEE, Vol. 2, pp. 28–28.
- 646 Chassignet, E. P., Hurlburt, H. E., Smedstad, O. M., Halliwell, G. R., Hogan, P. J., Wall-
 647 craft, A. J., Baraille, R., and Bleck, R. (2007). “The HYCOM (HYbrid Coordinate
 648 Ocean Model) data assimilative system,” Journal of Marine Systems **65**(1-4), 60–83, doi:
 649 [10.1016/J.JMARSYS.2005.09.016](https://doi.org/10.1016/J.JMARSYS.2005.09.016).
- 650 Chen, R., Poulsen, A., and Schmidt, H. (2019). “Spectral, spatial, and tem-
 651 poral characteristics of underwater ambient noise in the Beaufort Sea in 1994
 652 and 2016,” The Journal of the Acoustical Society of America **145**(2), 605–
 653 614, <https://asa.scitation.org/doi/full/10.1121/1.5088601http://files/757/>
 654 [Chenetal.-2019-Spectral,spatial,andspacecharacteristicsof.pdf](https://files/757/Chenetal.-2019-Spectral,spatial,andspacecharacteristicsof.pdf), doi: [10.1121/1.5088601](https://doi.org/10.1121/1.5088601).
- 655 Chen, R., and Schmidt, H. (2020). “Temporal and spatial charac-
 656 teristics of the Beaufort Sea ambient noise environment,” The Jour-

- 658 nal of the Acoustical Society of America **148**(6), 3928–3941, <https://doi.org/10.1121/10.0002955>
- 659 //asa.scitation.org/doi/full/10.1121/10.0002955http://files/755/
- 660 [ChenandSchmidt-2020-TemporalandspatialcharacteristicsoftheBeaufou.pdf](#), doi:
- 661 [10.1121/10.0002955](https://doi.org/10.1121/10.0002955).
- 662 Claus, B., Kepper, J. H., Suman, S., and Kinsey, J. C. (2018). “Closed-loop one-way-travel-
- 663 time navigation using low-grade odometry for autonomous underwater vehicles,” Journal
- 664 of Field Robotics **35**(4), 421–434, doi: [10.1002/rob.21746](https://doi.org/10.1002/rob.21746).
- 665 Council, N. R. (2011). *National Security Implications of Climate Change for U.S. Naval Forces* (The National Academies Press, Washington, DC), <https://www.nap.edu/catalog/12914/national-security-implications-of-climate-change-for-us-naval-forces>.
- 666 national-security-implications-of-climate-change-for-us-naval-forces.
- 667 Deffenbaugh, M. (1997). “Optimal Ocean Acoustic Tomography and Navigation with Moving Sources,” Ph.D. thesis, MIT-WHOI Joint Program in Oceanography/Applied Ocean
- 668 Science and Engineering.
- 669 Deffenbaugh, M., Bellingham, J. G., and Schmidt, H. (1996a). “Relationship between
- 670 spherical and hyperbolic positioning,” Oceans Conference Record (IEEE) **2**, 590–595, doi:
- 671 [10.1109/OCEANS.1996.568293](https://doi.org/10.1109/OCEANS.1996.568293).
- 672 Deffenbaugh, M., Schmidt, H., and Bellingham, J. G. (1996b). “Acoustic positioning in a
- 673 fading multipath environment,” in *OCEANS 96 MTS/IEEE Conference Proceedings. The*
- 674 *Coastal Ocean-Prospects for the 21st Century*, IEEE, Vol. 2, pp. 596–600.
- 675 Duda, T. F., Morozov, A. K., Howe, B. M., Brown, M. G., Speer, K., Lazarevich,
- 676 P., Worcester, P. F., and Cornuelle, B. D. (2006). “Evaluation of a long-range joint

- 680 acoustic navigation / thermometry system," in *Oceans 2006*, pp. 1–6, <http://files/939/Dudaetal.-2006-EvaluationofaLong-RangeJointAcousticNavigati.pdf> <http://files/940/4099137.html>, doi: [10.1109/OCEANS.2006.306999](https://doi.org/10.1109/OCEANS.2006.306999).
- 683 Duda, T. F., Zhang, W. G., and Lin, Y.-T. (2021). "Effects of Pacific Summer Water layer
684 variations and ice cover on Beaufort Sea underwater sound ducting," *The Journal of the
685 Acoustical Society of America* **149**(4), 2117–2136, doi: [10.1121/10.0003929](https://doi.org/10.1121/10.0003929).
- 686 Duda, T. F., Zhang, W. G., Lin, Y.-T., and Newhall, A. E. (2019). "Long-
687 range sound propagation in the Canada Basin," <http://files/565/Dudaetal.-Unknown-LONG-RANGESOUNDPROPAGATIONINTHECANADABASIN.pdf>.
- 689 Elisseeff, P., Schmidt, H., and Xu, W. (2002). "Ocean acoustic tomography as a data assimilation problem," *IEEE Journal of Oceanic Engineering* **27**(2), 275–282, <http://files/438/Elisseeff,Schmidt,Xu-2002-OceanAcousticTomographyasaDataAssimilationProblem.pdf>, doi: [10.1109/JOE.2002.1002482](https://doi.org/10.1109/JOE.2002.1002482).
- 694 Eustice, R. M., Whitcomb, L. L., Singh, H., and Grand, M. (2006). "Recent advances in
695 synchronous-clock one-way-travel-time acoustic navigation," *Oceans 2006* doi: [10.1109/OCEANS.2006.306931](https://doi.org/10.1109/OCEANS.2006.306931).
- 697 Eustice, R. M., Whitcomb, L. L., Singh, H., and Grund, M. (2007). "Experimental results in
698 synchronous-clock one-way-travel-time acoustic navigation for autonomous underwater vehicles," in *Proceedings - IEEE International
699 Conference on Robotics and Automation*, pp. 4257–4264, <http://files/877/Eusticeetal.-2007-ExperimentalResultsinSynchronous-ClockOne-Way-.pdf> <http://files/877/Eusticeetal.-2007-ExperimentalResultsinSynchronous-ClockOne-Way-.pdf>

- 702 [//files/878/4209752.html](http://files/878/4209752.html), doi: [10.1109/ROBOT.2007.364134](https://doi.org/10.1109/ROBOT.2007.364134).
- 703 Fossum, T. O., Norgren, P., Fer, I., Nilsen, F., Koenig, Z. C., and Ludvigsen, M. (2021).
- 704 “Adaptive sampling of surface fronts in the arctic using an autonomous underwater ve-
- 705 hicle,” IEEE Journal of Oceanic Engineering **46**(4), 1155–1164, doi: [10.1109/JOE.2021.3070912](https://doi.org/10.1109/JOE.2021.3070912).
- 706
- 707 Freitag, L., Ball, K., Partan, J., Koski, P., and Singh, S. (2016). “Long range acoustic
- 708 communications and navigation in the Arctic,” OCEANS 2015 - MTS/IEEE Washington
- 709 2–6, doi: [10.23919/oceans.2015.7401956](https://doi.org/10.23919/oceans.2015.7401956).
- 710 Graupe, C. E., Van Uffelen, L. J., Webster, S. E., Worcester, P. F., and Dzieci-
- 711 uch, M. A. (2019). “Preliminary results for glider localization in the Beau-
- 712 fort Duct using broadband acoustic sources at long range,” in *OCEANS 2019*
- 713 *MTS/IEEE Seattle, OCEANS 2019*, pp. 1–6, <http://files/763/Graupeetal.-2019-Preliminaryresultsforgliderlocalizationinthe.pdf>
- 714 <http://files/912/Graupeetal.-2019-Preliminaryresultsforgliderlocalizationinthe.pdf>
- 715
- 716 <http://files/764/8962637.html> <http://files/913/8962637.html>, doi: [10.23919/OCEANS40490.2019.8962637](https://doi.org/10.23919/OCEANS40490.2019.8962637).
- 717
- 718 Hayes, D. R., and Morison, J. H. (2002). “Determining turbulent vertical velocity, and
- 719 fluxes of heat and salt with an autonomous underwater vehicle,” Journal of Atmospheric
- 720 and Oceanic Technology **19**(5), 759–779.
- 721 Howe, B. M., Miksis-Olds, J., Rehm, E., Sagen, H., Worcester, P. F., and Haral-
- 722 abus, G. (2019). “Observing the Oceans Acoustically,” Frontiers in Marine Science **6**,
- 723 426, <https://www.frontiersin.org/article/10.3389/fmars.2019.00426/full>, doi:

724 10.3389/fmars.2019.00426.

725 Jackson, E. (1983). “Autonomous remotely controlled submersible “ARCS”,” in *Proceedings*
 726 of the 1983 3rd International Symposium on Unmanned Untethered Submersible Technol-
 727 ogy, IEEE, Vol. 3, pp. 77–88.

728 Jakuba, M. V., Roman, C. N., Singh, H., Murphy, C., Kunz, C., Willis, C., Sato,
 729 T., and Sohn, R. A. (2008). “Long-baseline acoustic navigation for under-ice
 730 autonomous underwater vehicle operations,” *Journal of Field Robotics* **25**(11-12),
 731 861–879, <https://onlinelibrary.wiley.com/doi/full/10.1002/rob.20250>
 732 <https://onlinelibrary.wiley.com/doi/abs/10.1002/rob.20250>
 733 <https://onlinelibrary.wiley.com/doi/10.1002/rob.20250>, doi: 10.1002/ROB.20250.

734 Kepper, J. H., Claus, B. C., and Kinsey, J. C. (2017). “MEMS IMU and one-
 735 way-travel-time navigation for autonomous underwater vehicles,” in *OCEANS*
 736 2017 - Aberdeen, Vol. 2017-Octob, pp. 1–9, <http://files/550/Kepper,Claus,Kinsey-2017-MEMSIMUandOne-Way-Travel-TimeNavigationforAutonomousUnderwaterVehicles.pdf>,
 738 doi: 10.1109/OCEANSE.2017.8084842.

739 Krishfield, R., Toole, J., Proshutinsky, A., and Timmermans, M. L. (2008). “Automated
 740 ice-tethered profilers for seawater observations under pack ice in all seasons,” *Journal of*
 741 *Atmospheric and Oceanic Technology* **25**(11), 2091–2105, doi: 10.1175/2008JTECH0587.
 742 1.

743 Kukulya, A., Plueddemann, A., Austin, T., Stokey, R., Purcell, M., Allen, B., Littlefield, R.,
 744 Freitag, L., Koski, P., Gallimore, E. et al. (2010). “Under-ice operations with a remus-100
 745 auv in the arctic,” in *2010 IEEE/OES Autonomous Underwater Vehicles*, IEEE, pp. 1–8.

- 746 Kunz, C., Murphy, C., Camilli, R., Singh, H., Bailey, J., Eustice, R., Jakuba, M., Nakamura,
 747 K., Roman, C., Sato, T., Sohn, R., and Willis, C. (2008). “Deep sea underwater robotic
 748 exploration in the ice-covered Arctic ocean with AUVs,” in *2008 IEEE/RSJ International
 749 Conference on Intelligent Robots and Systems*, IEEE, pp. 3654–3660, <http://files/875/Kunzetal.-2008-Deepseaunderwaterroboticexplorationintheice.pdf>
 750 <http://files/968/Kunzetal.-2008-Deepseaunderwaterroboticexplorationintheice.pdf>
 751 <http://ieeexplore.ieee.org/document/4651097/>, doi: [10.1109/IROS.2008.4651097](https://doi.org/10.1109/IROS.2008.4651097).
- 753
- 754 Light, R., and Morison, J. (1989). “The autonomous conductivity-temprtture vehicle: First
 755 in the seashuttle family of autonomous underwater vehicle’s for scientific payloads,” in
 756 *Proceedings OCEANS*, Vol. 3, pp. 793–798, doi: [10.1109/OCEANS.1989.586683](https://doi.org/10.1109/OCEANS.1989.586683).
- 757 Litvak, A. (2015). “Acoustics of the deepwater part of the arctic ocean and of russia’s
 758 arctic shelf,” Herald of the Russian Academy of Sciences **85**, 239–250, doi: [10.1134/S1019331615030144](https://doi.org/10.1134/S1019331615030144).
- 760 Mikhalevsky, P. N., Sperry, B. J., Woolfe, K. F., Dzieciuch, M. A., and Worces-
 761 ter, P. F. (2020). “Deep ocean long range underwater navigation,” The Jour-
 762 nal of the Acoustical Society of America **147**(4), 2365–2382, <http://asa.scitation.org/doi/10.1121/10.0001081>
 763 <http://files/631/Mikhalevskyetal.-2020-Deepoceanlongrangeunderwaternavigation.pdf>, doi: [10.1121/10.0001081](https://doi.org/10.1121/10.0001081).
- 764
- 765 Norgren, P., Lubbad, R., and Skjetne, R. (2014). “Unmanned underwater vehicles in Arctic
 766 operations,” in *22nd IAHR International Symposium on Ice*.

- 767 Paull, L., Saeedi, S., Seto, M., and Li, H. (2014). *AUV navigation and*
 768 *localization: A review*, **39**, pp. 131–149, <http://files/127/Paulletal.-2014-AUVnavigationandlocalizationAreview.pdf>.
- 770 Plueddemann, A. J., Kukulya, A. L., Stokey, R., and Freitag, L. (2012). “Autonomous
 771 Underwater Vehicle Operations Beneath Coastal Sea Ice,” IEEE/ASME Transactions
 772 on Mechatronics **17**(1), 54–64, doi: [10.1109/TMECH.2011.2174798](https://doi.org/10.1109/TMECH.2011.2174798) conference Name:
 773 IEEE/ASME Transactions on Mechatronics.
- 774 Porter, M. B. (2011). “The BELLHOP Manual and User’s Guide,” HLS Research, , 2010
 775 1–57, <http://oalib.hlsresearch.com/Rays/HLS-2010-1.pdf>.
- 776 Poulsen, A. J., and Schmidt, H. (2017). “Acoustic noise properties in the rapidly changing
 777 Arctic Ocean,” **070005**(2016), 070005, doi: [10.1121/2.0000552](https://doi.org/10.1121/2.0000552).
- 778 Randeni, S., Schneider, T., and Schmidt, H. (2020). “Construction of a
 779 high-resolution under-ice AUV navigation framework using a multidisci-
 780 plinary virtual environment,” in *2020 IEEE/OES Autonomous Underwater
 781 Vehicles Symposium, AUV 2020*, pp. 1–7, <http://files/689/Randenietal.-2020-Constructionofahigh-resolutionunder-iceAUVna.pdf>, doi: [10.1109/AUV50043.2020.9267950](https://doi.org/10.1109/AUV50043.2020.9267950).
- 784 Randeni, S., Schneider, T., Schmidt, H., Bhatt, E., and Viquez, O. (2021). “A high-
 785 resolution AUV navigation framework with integrated communication and tracking for
 786 under-ice deployments,” *Field Robotics* (in review).
- 787 Rossby, T., Dorson, D., and Fontaine, J. (1986). “The RAFOS System,” *Journal of Atmo-*
 788 *spheric and Oceanic Technology* **3**, 148–162.

- 789 Rypkema, N. R., Fischell, E. M., and Schmidt, H. (2017). “One-Way Travel-Time Inverted
 790 Ultra-Short Baseline Localization for Low-Cost Autonomous Underwater Vehicles,” in *2017*
 791 *IEEE International Conference on Robotics and Automation (ICRA)*, Singapore, pp. 4920–
 792 4926.
- 793 Schmidt, H., and Schneider, T. (2016). “Acoustic communication and navigation in
 794 the new Arctic-A model case for environmental adaptation,” 3rd Underwater Com-
 795 munications and Networking Conference, Ucomms 2016 <http://files/583/Schmidt,Schneider-2016-AcousticCommunicationandNavigationintheNewArctic-AModelCaseforEnvironment.pdf>, doi: [10.1109/UComms.2016.7583469](https://doi.org/10.1109/UComms.2016.7583469).
- 798 Schneider, T., and Schmidt, H. (2018). “NETSIM: A realtime virtual ocean hardware-
 799 in-the-loop acoustic modem network simulator,” in *2018 4th Underwater Communi-*
 800 *cations and Networking Conference, UComms 2018*, pp. 1–5, <http://files/1047/SchneiderandSchmidt-2018-NETSIMARealtimeVirtualOceanHardware-in-the-l.pdf>, doi: [10.1109/UComms.2018.8493188](https://doi.org/10.1109/UComms.2018.8493188).
- 803 Schneider, T., Schmidt, H., and Randeni, S. (2020). “Self-Adapting Under-Ice Inte-
 804 grated Communications and Navigation Network,” 2020 5th Underwater Communica-
 805 tions and Networking Conference, UComms 2020 5, <http://files/607/Schneideretal.-Self-AdaptingUnder-IceIntegratedCommunications.pdf>.
- 807 Singh, S., Grand, M., Bingham, B., Eustice, R., Singh, H., and Freitag, L. (2006).
 808 “Underwater acoustic navigation with the WHOI Micro-Modem,” in *Oceans 2006*,
 809 IEEE, pp. 1–4, <http://ieeexplore.ieee.org/document/4099008/>, doi: [10.1109/OCEANS.2006.1650001](https://doi.org/10.1109/OCEANS.2006.1650001).
 810 [Singhetal.-2006-UnderwaterAcousticNavigationwiththeWHOIMicro.pdf](http://files/774/Singhetal.-2006-UnderwaterAcousticNavigationwiththeWHOIMicro.pdf), doi: [10.1109/OCEANS.2006.1650001](https://doi.org/10.1109/OCEANS.2006.1650001).

811 1109/OCEANS.2006.306853.

812 Timmermans, M.-L., and Winsor, P. (2013). “Scales of horizontal density structure in the
813 chukchi sea surface layer,” Continental Shelf Research **52**, 39–45.

814 Toole, J. M., Krishfield, R. A., Timmermans, M. L., and Proshutinsky, A. (2011). “The
815 Ice-Tethered profiler: Argo of the Arctic,” Oceanography **24**(3), 126–135, doi: [10.5670/oceanog.2011.64](https://doi.org/10.5670/oceanog.2011.64).

817 Uffelen, L. J. V., Howe, B. M., Nosal, E.-M., Carter, G. S., Worcester, P. F., and Dzieciuch,
818 M. A. (2016). “Localization and subsurface position error estimation of gliders using
819 broadband acoustic signals at long range,” IEEE Journal of Oceanic Engineering **41**(3),
820 501–508.

821 Van Uffelen, L. J. (2021). “Global Positioning Systems: Over Land and Under Sea,” Acoustics
822 Today **17**(1), 52, doi: [10.1121/at.2021.17.1.52](https://doi.org/10.1121/at.2021.17.1.52).

823 Van Uffelen, L. J., Nosal, E.-M., Howe, B. M., Carter, G. S., Worcester, P. F., Dzieciuch,
824 M. A., Heaney, K. D., Campbell, R. L., and Cross, P. S. (2013). “Estimating uncertainty
825 in subsurface glider position using transmissions from fixed acoustic tomography sources,”
826 The Journal of the Acoustical Society of America **134**(4), 3260–3271, doi: [10.1121/1.4818841](https://doi.org/10.1121/1.4818841).

828 Webster, S. E., Eustice, R. M., Singh, H., and Whitcomb, L. L. (2009). “Preliminary
829 deep water results in single-beacon one-way-travel-time acoustic navigation
830 for underwater vehicles,” 2009 IEEE/RSJ International Conference on Intelligent
831 Robots and Systems, IROS 2009 2053–2060, <http://files/416/Websteretal.-2009-Preliminarydeepwaterresultsinsingle-beaconone-way-travel-timeacousticnavigationf>

- 833 pdf, doi: [10.1109/IROS.2009.5354457](https://doi.org/10.1109/IROS.2009.5354457).
- 834 Webster, S. E., Eustice, R. M., Singh, H., and Whitcomb, L. L. (2012). “Advances in
835 single-beacon one-way-travel-time acoustic navigation for underwater vehicles,” Interna-
836 tional Journal of Robotics Research **31**(8), 935–950, doi: [10.1177/0278364912446166](https://doi.org/10.1177/0278364912446166).
- 837 Webster, S. E., Freitag, L. E., Lee, C. M., and Gobat, J. I. (2015). “Towards real-time
838 under-ice acoustic navigation at mesoscale ranges,” in *Proceedings - IEEE International
839 Conference on Robotics and Automation*, June, IEEE, pp. 537–544, [http://files/625/
840 Websteretal.-2015-Towardsreal-timeunder-iceacousticnavigationat.pdf](http://files/625/Websteretal.-2015-Towardsreal-timeunder-iceacousticnavigationat.pdf) <http://files/641/Websteretal.-2015-Towardsreal-timeunder-iceacousticnavigationat.pdf>
841 <http://files/835/Websteretal.-2015-Towardsreal-timeunde>, doi: [10.1109/ICRA.2015.7139231](https://doi.org/10.1109/ICRA.2015.7139231).
- 842 Wu, M., Barmin, M. P., Andrew, R. K., Weichman, P. B., White, A. W., Lavely, E. M.,
843 Dzieciuch, M. A., Mercer, J. A., Worcester, P. F., and Ritzwoller, M. H. (2019).
844 “Deep water acoustic range estimation based on an ocean general circulation model:
845 Application to PhilSea10 data,” The Journal of the Acoustical Society of America
846 **146**(6), 4754–4773, [https://asa.scitation.org/doi/10.1121/1.5138606](https://doi.org/10.1121/1.5138606) <http://files/947/Wuetal.-2019-Deepwateracousticrangeestimationbasedonano.pdf>
847 <http://files/948/1.html>, doi: [10.1121/1.5138606](https://doi.org/10.1121/1.5138606).
- 848
- 849
- 850